Original Article

Parameter identification of crack-like notches in aluminum plates based on strain gauge data

Ramdane Boukellif(iD), Andreas Ricoeur and Matthias Oxe

Abstract
The identification of crack parameters and stress intensity factors in aluminum plates under tensile loading is in the focus of the presented research. In this regard, data of strain gauges, distributed along the edges of the samples, are interpreted. In the experiments, slit-shaped notches take the role of cracks located in the interior of the specimens. Their positions, inclinations and lengths as well as the magnitudes of external loadings are identified solving the inverse problems of cracked plates and associated strain fields. Exploiting the powerful approach of distributed dislocations, based on Green's functions provided by the framework of linear elasticity, in conjunction with a genetic algorithm, allows for a very efficient identification of the sought parameters, thus being suitable for in situ monitoring of engineering structures. Tested samples exhibit one or two straight crack-like notches as well as a kinked one.

Introduction

The monitoring of cracks in engineering structures is an essential issue within concepts of maintenance and reliable operation. In particular, light weight design in this context requires a smart interplay of numerical prediction and periodical inspection. More sophisticated concepts involve in situ monitoring of structures, being particularly challenging at long-term surveys, under harsh environmental conditions or at locations being difficult to access. Simple and robust sensing devices requiring little technical equipment are beneficial against this background, not to mention the economic aspect.

Classical strain gauges applied to the surface of a structure certainly satisfy these requirements, providing reliable data of local strain in the long term. In contrast to embedded techniques, where sensing devices are a priori integrated into structures,[1,2] surface-based solutions are more flexible on the one hand. On the other, strain gauges are exposed to environmental influences and provide only two-dimensional data, while embedded sensors allow reconstruction of 3D information. Strain fields nowadays are successfully measured by Digital Image Correlation (DIC), providing continuous 3D strain data of a selected part of a surface. A related optical approach denoted as Direct Deformation Estimation (DDE)[3] efficiently detects local strain concentrations and the onset of fracture. Going along with extended technical equipment DIC is, however, barely suitable for in-service monitoring of engineering structures, but rather designed for laboratory experiments. Techniques based for example, on Lamb wave reflection and scattering at crack faces[4,5] are well-established and reliably provide information on positions and lengths of cracks. The same basically holds for yet less established approaches, for example, interpreting changes in electrical resistivity in conducting structures due to cracks.[6] The identification of crack tip loading quantities such as stress intensity factors (SIF), however, is beyond their scope and inevitably requires information on either the magnitude of remote loading or on local relative displacements induced by cracks in a loaded structure.

Institute of Mechanics, University of Kassel, Kassel, Germany

Corresponding author:
Ramdane Boukellif, Institute of Mechanics, University of Kassel, Kassel 34125, Germany.
Email: ramdane.boukellif@uni-kassel.de

Besides the positions and lengths of cracks, the crack tip loading in terms of SIF constitutes precious information for the assessment of the risk potential of a crack and the prediction of residual life time of the structural component. Thus, on the one hand, strains have to be monitored with sufficient accuracy and at sufficiently many positions within an area prone to cracking. On the other hand, the relation of crack parameters, loading, and strain fields has to be known. In this context, closed-form solutions are preferable, however not available for even single straight cracks in bounded structures. Pure numerical solutions, for example, based on the finite element or related methods and discretization schemes, respectively, have the disadvantages of less flexibility, expensive model generation and computation, in particular concerning the inverse problem of parameter identification, and big data.

Semi-analytical approaches to strain fields of single or multiple cracks, in connection with a robust algorithm of parameter identification, are thus beneficial with regard to the intended application. Within the context of solid mechanics, shells and plates are the relevant 2D elements modeling light weight structures to be monitored with this concept. Considering a rectangular plate as a cutout of a thin structure, as depicted in Figure 1, shear and normal tractions $\overline{\sigma}_{ij}$ at its edges replace the local internal specific forces of the structure constituting boundary loads of a sub-model containing the crack(s). The small colored quadratic areas in the sketch indicate possible positions of strain gauges. To interpret strain data in terms of crack parameters, boundary loads, and finally SIF, the cracked plate problem of Figure 1 has to be solved based on a preferably semi-analytical approach.

In this work, the distributed dislocation technique (DDT) of linear elasticity[7-9] is applied to calculate the remote strain fields at different positions in plates containing one or multiple cracks and plates with kinked cracks under mixed-mode loading conditions. The power of this method lies in its efficiency due to the fact that just boundaries have to be discretized; however, compared with the boundary element method, the DDT exhibits a more pronounced analytical background. Consequently, the solutions for the stress and displacement fields are calculated for arbitrary geometries based on closed-form solutions of single dislocations[10] and rudimentary numerical integration. A further advantage is that the stress singularity at the crack tip is calculated accurately. Various crack problems have so far been treated applying the DDT.[11-20]

Several works on strain-based crack parameter identification have been published in the last two decades. Maheshwari et al.[21] investigate an approach to health monitoring of structures using multiple smart materials. Liang and Hwu[22] use an artificial neural network for the on-line identification of holes and cracks in composite structures and Hattori and Sáez[23] for crack identification in magnetoelectroelastic materials. The boundary element method is applied to solve finite domain problems for the identification of holes and cracks in circular piezoelectric plates.[24] Hwu and Liang[25] and Liang and Sun[26] theoretically and experimentally investigate the identification of holes and cracks in composite plates for multiple static loading modes using strain gauges and Hardware-In-The-Loop Simulations. Again, the boundary element method is applied here to solve the direct problem and nonlinear optimization is adopted for the inverse problem. There are also several works on crack detection using the XFEM to solve the direct problem and, for example, the genetic algorithm for solving the inverse problem in the sense of a parameter optimization.[27-30] Gadala and McCullough[31] realize the solution of the direct problem by the FEM. The method of proper orthogonal decomposition (POD) is also used to solve inverse crack problems.[32-34]

Electric signals from a polymeric piezoelectric foil attached to the surface of the structure are interpreted by Bäcker et al.[35] The crack tip near-field is used for crack parameter and SIF identification. One disadvantage of this approach is that a comprehensive grid of measuring points is required to be sufficiently close to any position of the crack tip. Just very recently an edge crack was monitored experimentally by strain sensors, also exploiting the near-tip fields.[36] Complex, in particular multiple crack and inclined center crack, problems are proclaimed as future targets in this work. Boukellif and Ricoeur[37] numerically and experimentally realized a sensor concept, applying the body force method to infinite and semi-infinite plate structures with single cracks and exploiting strain data far from the crack. The inverse problem is solved applying the particle swarm optimization (PSO) algorithm. The number of unknowns to be determined, however, is comparably small, unless restricting to the simple case of a Griffith crack. In a recent work, Boukellif and Ricoeur[38] use the DDT for the identification of crack parameters and SIF based on numerical experiments, assuming finite and semi-infinite plates with one or multiple center or edge cracks. A kinked crack is subject to parameter identification based on numerical strain data, and an inclined center crack is investigated experimentally, solving inverse problems with a genetic algorithm.[39]

In this work, a monitoring concept of cracks providing positions, inclinations, and lengths as well as SIF based on data of 8 to 12 strain gauges distributed along
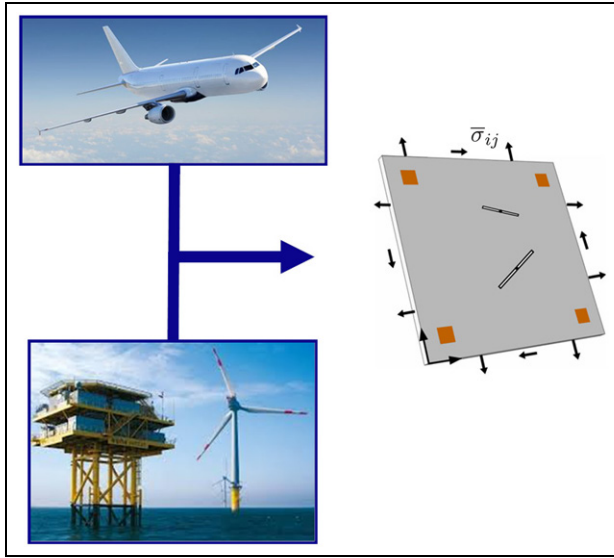
Figure 1. Examples of engineering structures to be modeled with plates or shells and rectangular plate model with two cracks and boundary tractions $\overline{\sigma}_{ij}$, constituting the reduced problem to be solved as a theoretical basis of experimental identification of crack and loading parameters.

the edges of a rectangular plate is verified experimentally. The high efficiency of the concept is essentially due to the semi-analytical approach of distributed dislocations representing cracks and external boundaries. The concept has been elaborated and verified previously, however just theoretically, taking numerical strain data as a basis.[38] It was investigated, among other things, to which extent measuring errors have an impact on the accuracy of parameter identification or how the number of gauges affects the results. A verification of the findings in the laboratory has been pending so far. Due to manufacturing issues, cracks are replaced by slim notches in the experiment.

Theoretical framework

In this section, the theoretical background of the approach, relating crack parameters and loads on the one hand and the strain field on the other, is outlined in brief. A detailed depiction is found in a recent work.[38]

The direct problem is solved by using the distributed dislocations method. The Green's function G_{ijk} is the basis to calculate the stress fields due to one dislocation in an infinite body.[10] It is also used to model boundaries of a finite body and straight cracks (see Figure 2) or kinked cracks (see Figure 3). Applying the superposition principle and using suitable boundary conditions, a finite body with cracks is cut out of an infinite plane. This is done by distributing the dislocation densities along the outer edges and crack faces.[38]

According to Figures 2 and 3 and using the principle of linear superposition, the stresses induced on the I-th boundary or crack line, that is, $I \in [I_b, I_c]$, due to the distributions of dislocations on all boundaries and cracks located at $\hat{\xi}_J$ are calculated in local coordinates as

$$
\begin{bmatrix} \sigma_{\hat{x}\hat{x}}^{D;I}(\hat{x}_I) \\ \sigma_{\hat{y}\hat{y}}^{D;I}(\hat{x}_I) \\ \sigma_{\hat{x}\hat{y}}^{D;I}(\hat{x}_I) \end{bmatrix} = \frac{2\mu}{\pi(\kappa+1)} \sum_{J=1}^{M}
$$

$$
\int_{-a_J}^{a_J} \begin{bmatrix} G_{\hat{x}\hat{x}\hat{x}}^{IJ}(\hat{x}_I;\hat{\xi}_J) & G_{\hat{y}\hat{x}\hat{x}}^{IJ}(\hat{x}_I;\hat{\xi}_J) \\ G_{\hat{x}\hat{y}\hat{y}}^{IJ}(\hat{x}_I;\hat{\xi}_J) & G_{\hat{y}\hat{y}\hat{y}}^{IJ}(\hat{x}_I;\hat{\xi}_J) \\ G_{\hat{x}\hat{x}\hat{y}}^{IJ}(\hat{x}_I;\hat{\xi}_J) & G_{\hat{y}\hat{x}\hat{y}}^{IJ}(\hat{x}_I;\hat{\xi}_J) \end{bmatrix} \begin{bmatrix} B_{\hat{x}}(\hat{\xi}_J) \\ B_{\hat{y}}(\hat{\xi}_J) \end{bmatrix} d\hat{\xi}_J \quad (1)
$$

$$
|\hat{x}_I| < a_I, I = 1, ..., M
$$

where $M = M_b + M_c$ comprises all boundaries and cracks of lengths $2a_{Ib}$ and $2a_{Ic}$. Kolosov's constant κ is related to Poisson's ratio ν as $\kappa = (3 - \nu)/(1 + \nu)$ for plane stress
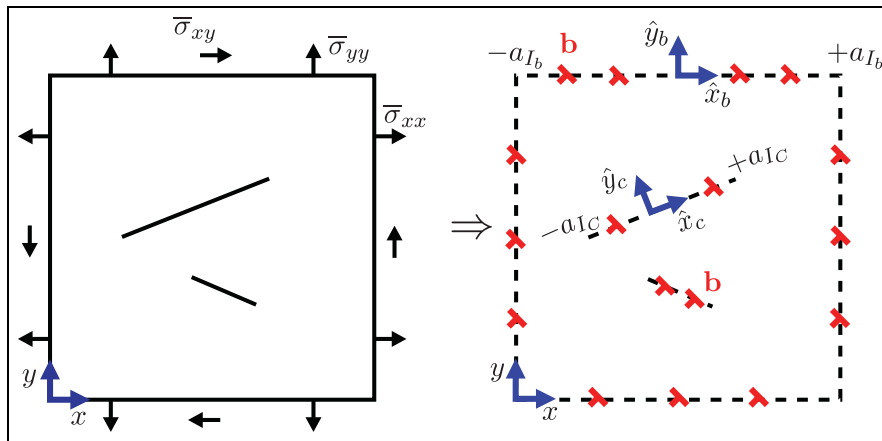

Figure 2. Finite plate with two cracks as an example of how to apply dislocations to model free surfaces.[38]
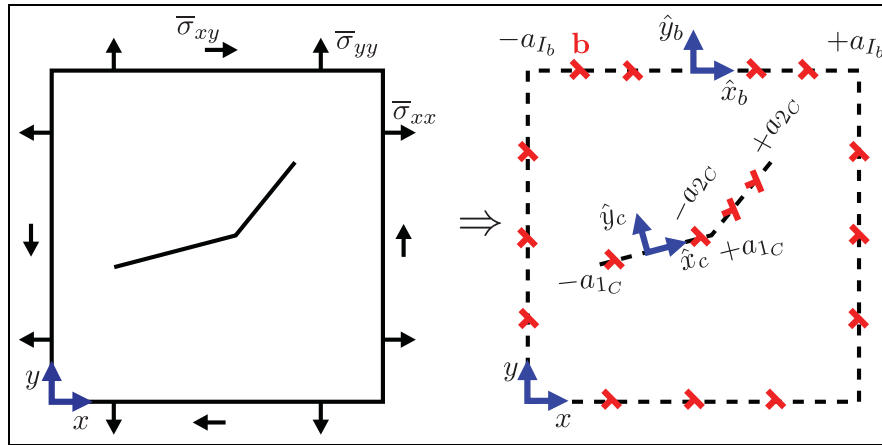
Figure 3. Kinked crack in a finite plate and distributed dislocations substituting internal and external boundaries.

and $\kappa = 3 - 4\nu$ for plane stain and μ denotes the shear modulus.

The dislocations **b**, indicated in the figures, have been replaced by dislocation densities $B_{\hat{x},\hat{y}}$ following the relation

$$d\hat{\mathbf{b}} = \begin{pmatrix} db_{\hat{x}} \\ db_{\hat{y}} \end{pmatrix} = \begin{pmatrix} B_{\hat{x}}(\hat{\xi})d\hat{\xi} \\ B_{\hat{y}}(\hat{\xi})d\hat{\xi} \end{pmatrix} \tag{2}$$

The dislocation density $B_{\hat{x},\hat{y}}(\hat{\xi})$ in equation (1) is determined by suitable selection of the conditions at the boundaries and at the crack faces in terms of stresses $\sigma_{ij}^{D;I}$ ($ij = \hat{x}\hat{x}, \hat{y}\hat{y}, \hat{x}\hat{y}$). This leads to singular integral equations of the first kind with Cauchy kernel. These are solved by using Gauss-Chebyshev numerical quadrature, whereby the dislocation density is replaced by the product of two functions $w(\hat{s}_J = \hat{\xi}_J/a_J)$ and $\phi_{\hat{x}/\hat{y}}(\hat{s}_J)$. The fundamental solution $w(s)$ is given and the functions $\phi_{\hat{x}/\hat{y}}(s)$ are determined using the boundary conditions.

Figure 3 depicts a kinked crack in a plate. The stress conditions at the external boundaries and at cracks are the same as in Figure 2. In contrast to the problem of two distinct cracks, where the conditions

$$\int_{-1}^{1} B_i(s_1)ds_1 = 0 \tag{3}$$

$$\int_{-1}^{1} B_i(s_2)ds_2 = 0 \tag{4}$$

($i = \hat{x}, \hat{y}$) guarantee that the displacement jumps at all four crack tips vanish, the kinked crack satisfies the condition

$$\int_{-1}^{1} B_i(s_1)ds_1 + \int_{-1}^{1} B_i(s_2)ds_2 = 0 \tag{5}$$

The additional equation at the kink is that the values of the dislocation densities are equal there for both segments involved, that is

$$B_i(s_1 = +a_{1_c}) = B_i(s_2 = -a_{2_c}) \tag{6}$$

As soon as the functions $\phi_{\hat{x}/\hat{y}}(\hat{s}_J)$ are determined from equations (1) and (3) (one crack), or (1), (3) and (4) (two cracks), or (1), (5) and (6) (kinked crack), the stresses at arbitrary points can be calculated according to

$$\begin{bmatrix} \sigma_{xx}(x,y) \\ \sigma_{yy}(x,y) \\ \sigma_{xy}(x,y) \end{bmatrix} = \frac{2\mu}{\pi(\kappa+1)} \sum_{J=1}^{M} a_J \sum_{i=1}^{N} \frac{1}{N}$$

$$\begin{bmatrix} G_{xxx}^J(x,y;s_i^J) & G_{yxx}^J(x,y;s_i^J) \\ G_{xyy}^J(x,y;s_i^J) & G_{yyy}^J(x,y;s_i^J) \\ G_{xxy}^J(x,y;s_i^J) & G_{yxy}^J(x,y;s_i^J) \end{bmatrix} \begin{bmatrix} \phi_x(s_i^J) \\ \phi_y(s_i^J) \end{bmatrix} \tag{7}$$

where all quantities have been transformed into the global coordinate system (x,y) and N is the number of the integration points. The SIF are calculated from the relations

$$K_I(\pm) = \pm\sqrt{\pi a}\frac{2\mu}{\kappa+1}\phi_y(\pm 1),$$

$$K_{II}(\pm) = \pm\sqrt{\pi a}\frac{2\mu}{\kappa+1}\phi_x(\pm 1) \tag{8}$$

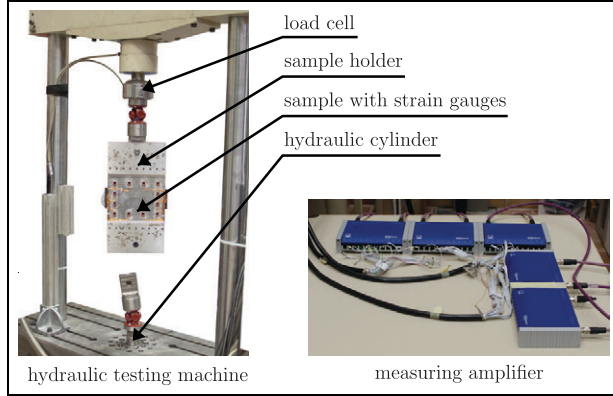The strain fields are calculated from equation (7) applying Hooke's law and assuming plane stress condition

Figure 4. Experimental setup for the measurement of strains in a plate specimen with one or two notches under uniaxial tensile loading.

Figure 5. Strain distribution ε_{yy} in an elastic plate (200 × 200 mm, plane stress condition, $E = 72000$ MPa, $\nu = 0.3$) with two notches and 12 virtual strain gauges under tensile stress determined from finite element simulation; sketch of one notch shows details.

$$
\begin{bmatrix}
\varepsilon_{xx}(x,y) \\
\varepsilon_{yy}(x,y) \\
\gamma_{xy}(x,y)
\end{bmatrix}
= \frac{1}{4\pi} \sum_{J=1}^{M} a_J \sum_{i=1}^{N} \frac{1}{N}
$$

$$
\cdot
\begin{bmatrix}
G_{xxx}^{J}(x,y;s_i^J) - \nu G_{xyy}^{J}(x,y;s_i^J) & G_{yxx}^{J}(x,y;s_i^J) - \nu G_{yyy}^{J}(x,y;s_i^J) \\
G_{xyy}^{J}(x,y;s_i^J) - \nu G_{xxx}^{J}(x,y;s_i^J) & G_{yyy}^{J}(x,y;s_i^J) - \nu G_{yxx}^{J}(x,y;s_i^J) \\
(1+\nu)G_{xxy}^{J}(x,y;s_i^J) & (1+\nu)G_{yxy}^{J}(x,y;s_i^J)
\end{bmatrix}
$$

$$
\begin{bmatrix}
\phi_x(s_i^J) \\
\phi_y(s_i^J)
\end{bmatrix}
\tag{9}
$$

Equation (9) is the basis of solving inverse problems, with measured strains as input data. A genetic algorithm (GA)[40] is applied therefore, allowing the identification of external loading, crack parameters, such as length, position or inclination angles, and the calculation of SIF. GA, as population based approaches and global optimizers, are nature-inspired search algorithms that emulate the Darwinian principle of "survival of the fittest" and may readily be applied to technical optimization problems.[41] The algorithm used is implemented in the software LS-OPT.

Experimental setup and results

In Figure 4, the experimental setup is presented, consisting of a uniaxial hydraulic testing machine, imposing a tensile load on the plate specimen, being connected to the machine by two sample holders.

The force is measured with a strain gauge load cell fixed to the one end of the sample, while the hydraulic power acts on the other. To prevent bending and torsional moments, each of the sample holders is connected to the testing machine by a cardanic joint. The specimen itself is firmly bolted with its holders, whereupon a milled groove guarantees a form-locked fixing
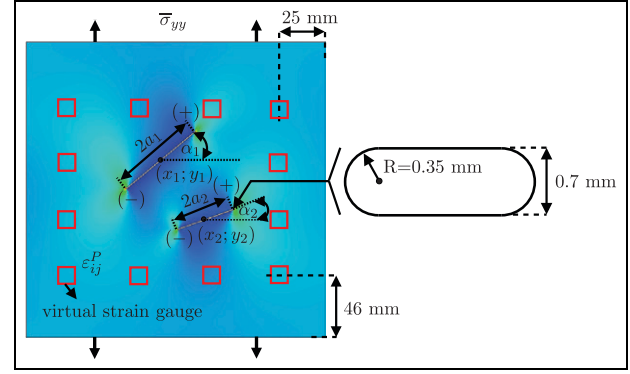
and homogeneous stress distributions at the loading edges. Five HBM multi-channel measuring amplifiers connected to a computer process the data of the 8 to 12 strain gauges applied to one of the specimen's largest surfaces.

Before evaluating experimental strain data, it has to be ensured that a notch of given width and a crack can be treated equivalently with respect to the intended parameter identification. Lacking the possibility of introducing sharp cracks in the interior of a plate, slender notches with a width of 0.4 mm have been manufactured instead by die-sinking or wire-cut electrical discharge machining (EDM). The solution of the inverse problem, on the other hand, is based on crack solutions emanating from the distributed dislocations technique, as depicted briefly in the previous section. In Figure 5, the finite element model of a plate with two slant notches of different inclinations and lengths under tensile stress is presented which has been used as an example for verification of the crack-notch analogy. Twelve virtual strain gauges, representing the locations where strains were sampled from the numerical solution, are arranged on a rectangular contour surrounding the notches. The width of the notches in the finite element simulation has been chosen 0.7 mm, thus being wider than the experimental notches. The results of parameter identification are given in Table 1.

Like in most of the following experiments, all three in-plane strain components have been evaluated at all 12 virtual gauge positions for the notched plate, however in this test taken from the finite element solution (see Figure 5). Just as in the experiments, the identification of the first nine parameters is based on the distributed dislocation technique in connection with the genetic algorithm assuming sharp cracks. It is

Table 1. Given (finite element method; notch) and identified (dislocation method; crack) parameters of the problem depicted in Figure 5.

Parameters	Given	Identified
$\overline{\sigma}_{yy}$ [MPa]	20	20.0
a_1 [mm]	30	30.45
α_1 [°]	40	40.13
x_1 [mm]	90	90.45
y_1 [mm]	120	120.09
a_2 [mm]	20	20.07
α_2 [°]	20	19.63
x_2 [mm]	120	119.5
y_2 [mm]	80	79.99
$K_I^{(1)}(+)$ [MPa $\sqrt{mm}$]	112.93	113.95
$K_I^{(1)}(-)$ [MPa $\sqrt{mm}$]	124.80	125.26
$K_{II}^{(1)}(+)$ [MPa $\sqrt{mm}$]	102.08	102.55
$K_{II}^{(1)}(-)$ [MPa $\sqrt{mm}$]	118.18	119.44
$K_I^{(2)}(+)$ [MPa $\sqrt{mm}$]	143.67	143.73
$K_I^{(2)}(-)$ [MPa $\sqrt{mm}$]	120.12	119.68
$K_{II}^{(2)}(+)$ [MPa $\sqrt{mm}$]	71.50	71.16
$K_{II}^{(2)}(-)$ [MPa $\sqrt{mm}$]	64.52	63.45

concluded that errors of the prediction are below 2%, although the notch width has been presumed almost double compared with the experimental condition, finally justifying the approach of treating notches as cracks. The SIF in the second column of Table 1 have been calculated for cracks, based on the given parameters of the notches listed above. The positive and negative signs in brackets distinguish the crack tips (see Figure 5).

Now coming to physical experiments, Figure 6 shows the one surface of a specimen, where strain gauges have been applied uniformly along the edges of a rectangle. This arrangement proved to be appropriate in various numerical experiments.[38] The rosettes enable the monitoring of all three in-plane strains, that is, ε_{xx},

ε_{yy}, and ε_{xy}. The size of the gauges being comparatively small, the area-averaged strain data can be assumed as local values with a vanishing error, which has been confirmed by numerical studies. The rectangular patterns on the specimen's surface are due to the milling process, reducing all plates from a thickness of originally 12 mm to the final 8 mm. The pattern is just an optical issue, the surface being mechanically smooth.

Particularly high demands have been made on the planarity of the sample, in order to avoid an in-plane bending moment perpendicular to the loading axis, generating different strain data on both surfaces. The quality of the manufacturing process has been verified a priori, applying strain gauges at corresponding positions on both sides of a test specimen, providing deviations of less than 2%. Due to the two through-length grooves along the loading edges, conceived for the sake of a homogeneous loading stress $\overline{\sigma}_{yy}$, the effective height of the sample is reduced by 2×5 mm.

In the first two specimens, the notch has been introduced by die-sinking EDM (Figures 6 and 8). More sophisticated notches were obtained by wire-cut EDM (Figures 9–11), where the notch faces are almost exactly parallel, whereas the die-sinking EDM produces slightly conical notches. The results of parameter identification of the sample depicted in Figure 6 are presented in Figure 7. The table shows the numerical quantity values of tensile loading stress $\overline{\sigma}_{yy}$, crack length a, inclination α and the center positions (x, y). To illustrate the quality of parameter identification, the sketch of the square with the included black and red lines indicates the given and the identified cracks. The errors in the stress, crack length, and inclination amount to 8%–9%, whereas the position is identified most accurately with a deviation of just 3.5%. The SIF at the positive and negative crack tips, predominantly depending on the parameters $\overline{\sigma}_{yy}$,
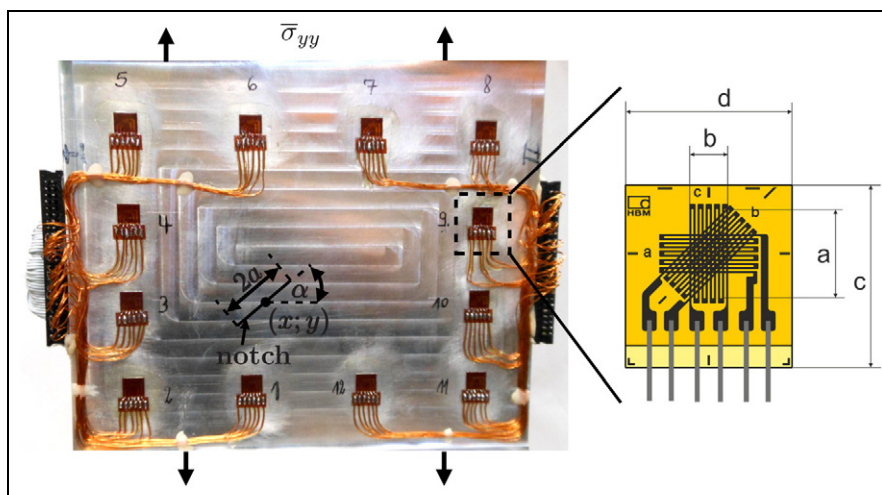

Figure 6. Specimen (Al-7075, $200 \times 200 \times 8$ mm) with one notch (15×0.4 mm) and 12 strain gauge rosettes ($a = 3$, $b = 1.3$, $c = 9$, $d = 9$ mm).[39]
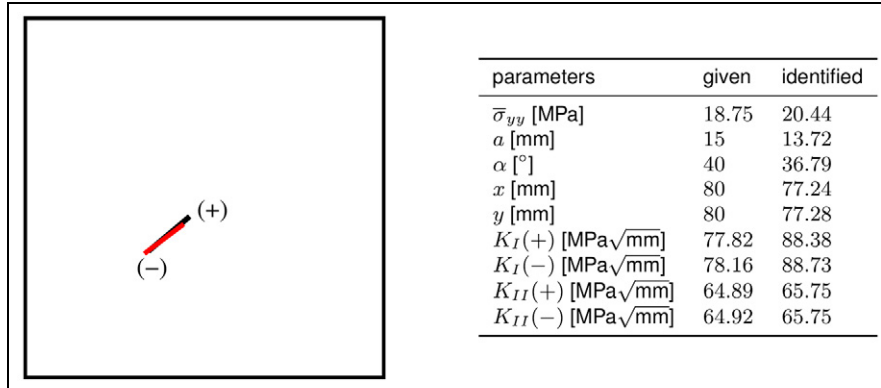
Figure 7. Parameter identification of the specimen in Figure 6; table shows the numerical values and sketch indicates the positions and lengths of given (black) and identified (red) cracks.
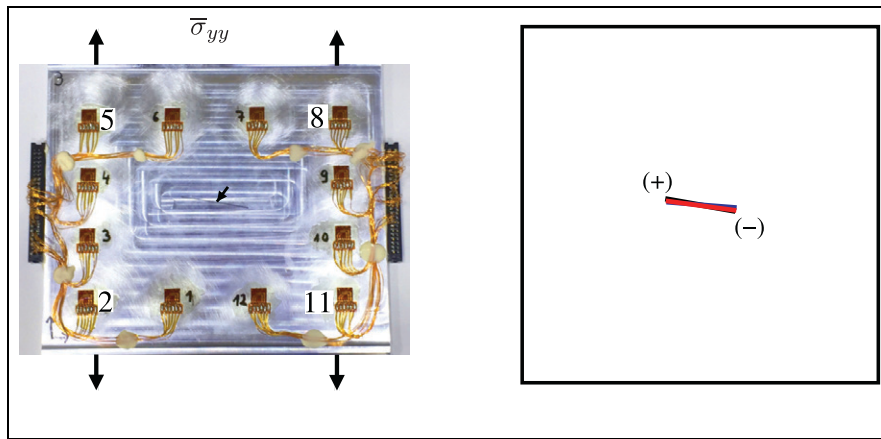
parameters	given	identified
$\overline{\sigma}_{yy}$ [MPa]	18.75	20.44
a [mm]	15	13.72
α [°]	40	36.79
x [mm]	80	77.24
y [mm]	80	77.28
$K_I(+)$ [MPa$\sqrt{\text{mm}}$]	77.82	88.38
$K_I(-)$ [MPa$\sqrt{\text{mm}}$]	78.16	88.73
$K_{II}(+)$ [MPa$\sqrt{\text{mm}}$]	64.89	65.75
$K_{II}(-)$ [MPa$\sqrt{\text{mm}}$]	64.92	65.75

Figure 8. Parameter identification with single crack/notch; sketch indicates the positions and lengths of given (black) and identified cracks with data from eight strain gauges No. 1, 3, 4, 6, 7, 9, 10, 12 evaluated (blue) and with data from all strain gauges (red).

a, and α, are identified very accurately for K_{II}, whereas the error of K_I amounts to 12%. The experiment has been repeated five times, as with all following specimens, producing strain data with negligible deviation.

Not withstanding their reproducibility, gauged strains are commonly known to exhibit errors of a few percent, just as positions of gauges do not exactly match their designated locations. Consequently, identified parameters cannot be expected to be as exact as predicted by numerical experiments.[38,39] The quality of parameter identification under real experimental conditions, as depicted in Figure 7, is considered to be reasonable, fully meeting engineering requirements of structural health monitoring.

In Figures 8 and 9, two more single crack/notch configurations with different positions, lengths, and inclinations are depicted, which have been tested with the same loading as in the previous example. The positions of strain gauges are identical for all the investigated samples in this work. Tables 2 and 3 show the given and identified parameters and associated relative errors

for the two specimens. The quality of the identifications is again illustrated by sketches in Figures 8 and 9. Accordingly, the crack/notch parameters as well as the loading stress have been determined even more accurately than for the first example in Figures 6 and 7. In particular, for the shorter crack close to the center of the plate in Figure 8, the parameters have been identified excellently. Evaluating the data of all 12 strain gauges, the load $\overline{\sigma}_{yy}$ exhibits by far the largest error amounting to 4%. Excluding the data from the gauges No. 2, 5, 8, 11 in the corner positions from the parameter identification still provides very good results. The fact that an array with eight gauges partly produces less error, for example, for the identified crack position (x, y), is not systematic due to the low absolute values, thus sparing interpretation. The longest crack of Figure 9 exhibits an excellent identification of the crack position, while errors in inclination, length, and the loading range from approximately 3% to 6%. Both crack tips are much closer to single strain gauges in this sample, thus strain gradients are larger there and the
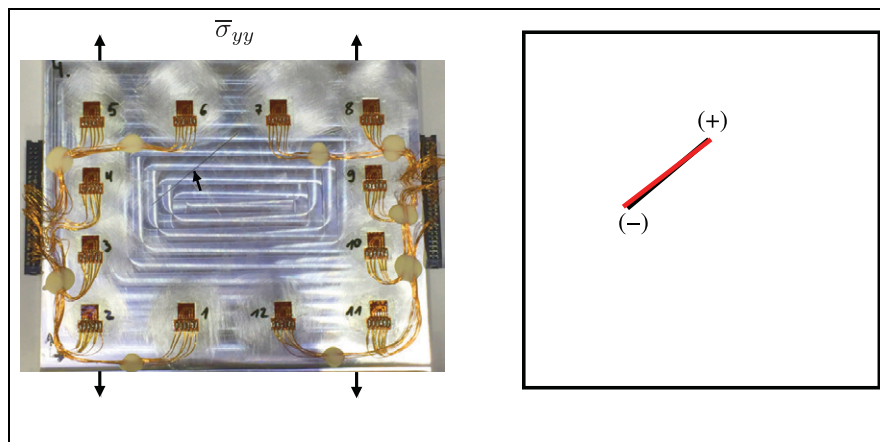
Figure 9. Parameter identification with single crack/notch; sketch indicates the positions and lengths of given (black) and identified (red) cracks.
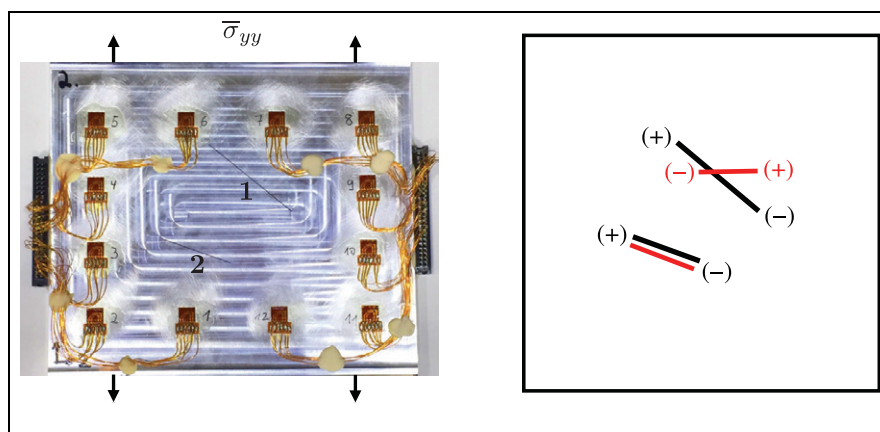

Figure 10. Parameter identification at a specimen with two cracks/notches; sketch indicates the positions and lengths of given (black) and identified (red) cracks.

accuracy of the gauging is supposed to be lower. In numerical experiments,[38,39] it was furthermore demonstrated that a sufficient distance of cracks and gauges improves the solution of the inverse problem. SIF are also well predicted in both samples, except for K_{II} in Table 2, which is due to the comparatively small absolute value of the predominantly mode-I loaded crack. In Table 3, the data of all 12 strain gauges have been evaluated, just as with the following sample.

In Figure 10, a two-crack problem is depicted with one longer notch (1) located close to the upper strain gauges and a shorter notch (2) below. The results of parameter identification are provided in Table 4 and the sketch of Figure 10. While the external loading and the parameters of crack (2) are reproduced well, in particular its inclination and horizontal position, the solution of the inverse problem yields a crack (1) exhibiting considerable deviations from the given one. Having a closer look at Table 4, the center position of the notch

is still reproduced well; however, the prediction of length and particularly inclination fails.

Figure 11 and Table 5 show the given and identified configurations of an angled crack/notch, consisting of two straight segments (1) and (2) connected by a sharp corner. While the loading quantity $\overline{\sigma}_{yy}$ again is identified very well, the predicted crack differs even qualitatively from the given one. In detail, the position of segment (1) and the inclination angle of segment (2) are fairly well reproduced, while the other parameters exhibit large deviations.

Obviously, specimens with more than one crack or crack segment cause problems in the parameter identification. However, it was demonstrated by means of virtual experiments,[38,39] where the data of strain gauges have been produced numerically as in Figure 5, that the approach applied here basically copes with even more complex multi-crack problems. A general conclusion, however, is that an increasing number of unknowns in

Table 2. Given and identified parameters of the sample in Figure 8 with 8 or 12 strain gauges evaluated.

Parameters	Given	Identified (8 strain gauges)	Error [%]	Identified (12 strain gauges)	Error [%]
$\overline{\sigma}_{yy}$ [MPa]	18.75	17.99	4.1	18.03	3.9
a [mm]	20	19.79	1.1	19.95	0.3
α [°]	170	175.53	3.3	172.23	1.3
x [mm]	100	100.07	0.07	100.49	0.5
y [mm]	100	100.01	0.01	99.66	0.3
$K_I(+)$ [MPa $\sqrt{\text{mm}}$]	152.37	148.81	2.33	148.06	2.83
$K_I(-)$ [MPa $\sqrt{\text{mm}}$]	152.37	148.81	2.33	148.07	2.82
$K_{II}(+)$ [MPa $\sqrt{\text{mm}}$]	−26.00	−10.99	-	−19.46	25
$K_{II}(-)$ [MPa $\sqrt{\text{mm}}$]	−26.00	−10.99	-	−19.44	25

Table 3. Given and identified parameters of the sample in Figure 9.

Parameters	Given	Identified	Error [%]
$\overline{\sigma}_{yy}$ [MPa]	18.75	17.59	6.3
a [mm]	30	31.09	3.5
α [°]	40	37.55	6.3
x [mm]	80	80.13	0.2
y [mm]	120	121.47	1.2
$K_I(+)$ [MPa $\sqrt{\text{mm}}$]	122.85	127.40	3.7
$K_I(-)$ [MPa $\sqrt{\text{mm}}$]	118.96	122.91	3.32
$K_{II}(+)$ [MPa $\sqrt{\text{mm}}$]	96.51	90.80	5.92
$K_{II}(-)$ [MPa $\sqrt{\text{mm}}$]	98.98	93.83	5.2

the inverse problem reduces the tolerance of the optimization algorithm with respect to random deviations of strain data from the given ones. The reason for the failure here thus must be attributed to the measuring errors introduced by the strain gauges.

Figure 12 confirms this statement, illustrating the strains at almost all gauge positions of the angled crack problem of Figure 11. The strain data of gauge No. 9 had to be excluded from the analysis due to technical problems. The numbers at the abscissa of Figure 12 consecutively label the strain components in the order

ε_{xx} for each of the 11 gauges, followed by ε_{xy} and finally ε_{yy} for all gauges. The black crosses and red dots in the graph correspond to the data of the given and identified crack, respectively. Both sets have been calculated with the distributed dislocation method. It is obvious that the strains of given and identified cracks are almost identical, exhibiting noteworthy relative deviations only for a few positions with predominantly small quantities. The same holds for the two-crack problem depicted in Figure 10, whereupon the respective analysis is not presented here. While in virtual experiments[38,39] these slight deviations apparently are allocated correctly, they are faded out by strain gauge signals. In Figure 13, the black crosses of Figure 12, corresponding to the given crack, are compared with measured strains. The error of the stain gauges obviously is larger than the differences in strains for the two-crack configurations; thus, an appropriate identification is not possible.

To cope with this problem, the arrangement of gauges might play a role. Numerical investigations indicate that a random distribution rather than a rectangular one effectuates a larger tolerance of the algorithm with respect to measuring errors. A further aspect is the nonlinear optimization applied to the inverse problem
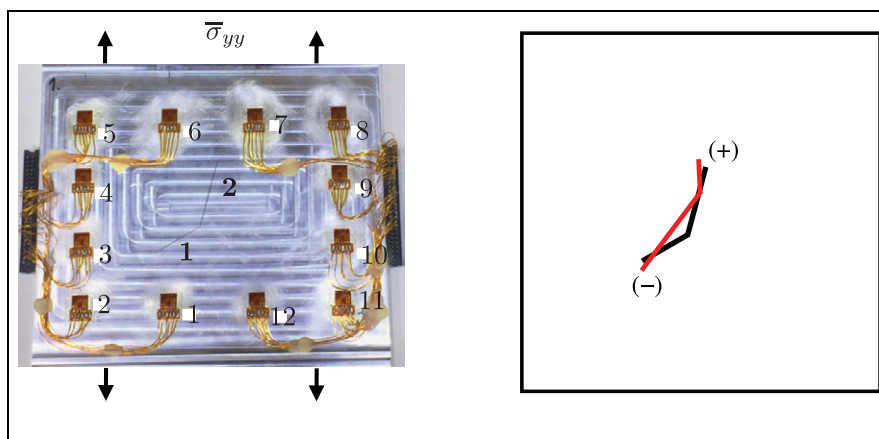

Figure 11. Parameter identification at a specimen with angled crack/notch consisting of two segments (1) and (2), numbers of strain gauges added to the photograph; sketch indicates the given (black) and identified (red) configurations.

Table 4. Given and identified parameters of the sample in Figure 10.

Parameters	Given	Identified	Error [%]
$\overline{\sigma}_{yy}$ [MPa]	18.75	19.86	2.8
a_1 [mm]	30	16.6	—
α_1 [°]	140	1	—
x_1 [mm]	110	114.23	3.8
y_1 [mm]	120	123.64	2.9
a_2 [mm]	20	19.15	4.3
α_2 [°]	160	159.2	0.5
x_2 [mm]	80	78.31	2.1
y_2 [mm]	80	75.01	6.4
$K_I^{(1)}(+)$ [MPa $\sqrt{mm}$]	107.09	154.48	-
$K_I^{(1)}(-)$ [MPa $\sqrt{mm}$]	118.23	145.97	-
$K_{II}^{(1)}(+)$ [MPa $\sqrt{mm}$]	−95.44	−4.31	-
$K_{II}^{(1)}(-)$ [MPa $\sqrt{mm}$]	−110.61	−7.60	-
$K_I^{(2)}(+)$ [MPa $\sqrt{mm}$]	135.21	145.13	7.34
$K_I^{(2)}(-)$ [MPa $\sqrt{mm}$]	113.03	136.33	18
$K_{II}^{(2)}(+)$ [MPa $\sqrt{mm}$]	−66.41	−61.35	7.62
$K_{II}^{(2)}(-)$ [MPa $\sqrt{mm}$]	−59.70	−59.30	0.67

Figure 12. Normal and shear strains at each gauge position for given and identified cracks in Figure 11, calculated with the dislocation method; numbers at abscissa start with ε_{xx} of gauges 1 to 12 indicated in Figure 11, followed by ε_{xy} and ε_{yy}, respectively, for gauges 1 to 12. Due to technical problems with gauge No. 9, these three strain data are not included.

Table 5. Given and identified parameters of the sample in Figure 11.

Parameters	Given	Identified	Error [%]
$\overline{\sigma}_{yy}$ [MPa]	18.75	18.71	0.2
a_1 [mm]	15	27.3	—
α_1 [°]	30	53	—
x_1 [mm]	80	83.02	3.7
y_1 [mm]	80	88.7	10.3
a_2 [mm]	20	9.6	—
α_2 [°]	45	39.8	12.3
$K_I(+)$ [MPa $\sqrt{mm}$]	2.67	7.28	-
$K_I(-)$ [MPa $\sqrt{mm}$]	130.79	72.31	-
$K_{II}(+)$ [MPa $\sqrt{mm}$]	2.18	9.03	-
$K_{II}(-)$ [MPa $\sqrt{mm}$]	79.27	100.82	-

Figure 13. Normal and shear strains for the problem in Figure 11 from experimental gauge measurements (red) and calculations with the dislocation method for the given crack (black); numbers at abscissa correspond to ε_{xx}, ε_{xy}, and ε_{yy} at gauge positions, following the order of Figure 12.

which has to be improved with regard to the identification of the objective function. Concerning engineering applications, the monitoring of crack growth typically emanates from a currently known situation, thus providing a unique target function.

Conclusion

Aluminum plates with slit-shaped notches of just a few tenths of a millimeter thickness have been investigated with the goal to identify the lengths, positions, and inclinations of the notches as well as the magnitudes of external loadings of the specimens based on data provided by arrays of strain gauges. It was proved by finite element simulation that the strain fields emanating
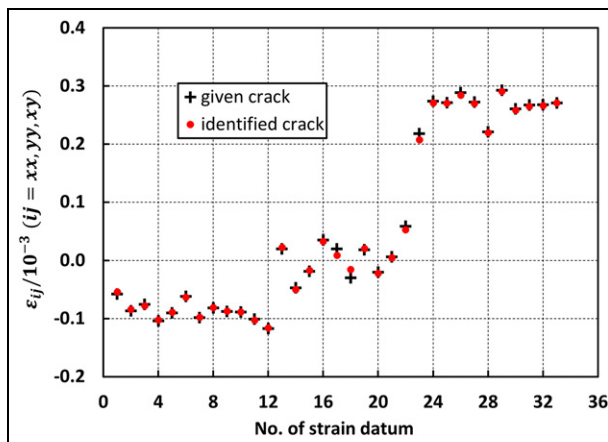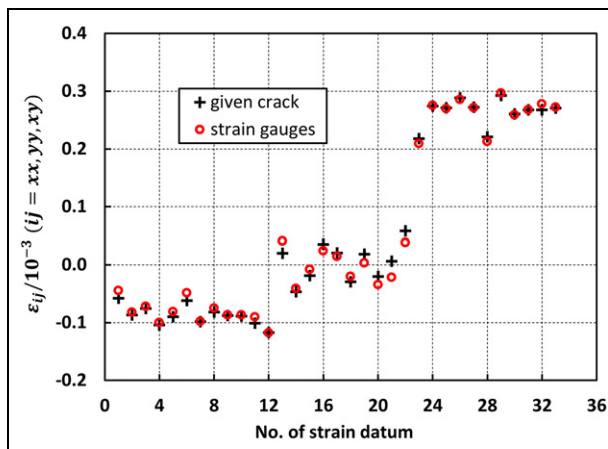
from the notches are almost identical to the ones induced by cracks of the same lengths and positions, given that gauges are being mounted sufficiently far from the notch or crack tips. The applied concept of solving the inverse problem of crack-induced strain fields, identifying both geometrical crack parameters and SIF based on the sophisticated mathematical-mechanical approach of the theory of distributed dislocations, has previously been investigated theoretically. The predicted efficiency and feasibility could be confirmed experimentally in this work, however reaching

its limits for two cracks or a kinked crack in one plate. Analyzing the associated strain fields of these particular samples theoretically by applying the method of distributed dislocations, and comparing the experimental strain data reveals two major issues. First of all, the strains at the positions of the gauges in these two cases are very similar for given and identified crack configurations, although the latter are apparently dissimilar. The errors of strain measurement, on the other hand, are larger than these deviations. Continuative theoretical investigations show that a modification of the positions of strain measurement, in such a way that gauges are distributed in a more disordered manner, might be a promising approach to cope with these problems, which appear to be characteristic for samples with multiple cracks or complex crack configurations.

Funding

ORCID iD

Ramdane Boukellif (iD) https://orcid.org/0000-0001-6789-7658

References

1. Giurgiutiu V. *Structural health monitoring with piezoelectric wafer active sensors*. 2nd ed. Cambridge, MA: Academic Press, 2014.
2. Tanaka N, Okabe Y and Takeda N. Temperature-compensated strain measurement using fiber Bragg grating sensors embedded in composite laminates. *Smart Mater Struct* 2003; 12: 940–946.
3. Boyle JJ, Kume M, Wyczalkowski MA, et al. Simple and accurate methods for quantifying deformation, disruption, and development in biological tissues. *J R Soc Interface* 2014; 11: 20140685.
4. Cho H and Lissenden CJ. Structural health monitoring of fatigue crack growth in plate structures with ultrasonic guided waves. *Struct Health Monit* 2012; 11(4): 393–404.
5. Zhao X, Kwan C and Luk KM. Wireless non-destructive inspection of aircraft wing with ultrasonic guided waves. In: *Proceedings of the 16th world conference on nondestructive testing*, Montreal, QC, Canada, 11 September 2004.
6. Armstrong TW and Sevostianov I. Electrical impedance changes due to cracks in planar conductive structural elements. *Struct Health Monit* 2015; 14: 489–501.
7. Bilby BA, Cottrell AH and Swinden KH. The spread of plastic yield from a notch. *Procee Royal Soci A* 1963; 272: 304–314.
8. Bilby BA and Eshelby JD. Dislocations and the theory of fracture. In: Liebowitz H (ed) *Fracture*. New York: Academic Press, 1968, pp. 99–182.
9. Weertman J. *Dislocation based fracture mechanics*. Aalto: World Scientific Publishing Co. Pte. Ltd, 1996.
10. Dundurs J and Mura T. Interaction between an edge dislocation and a circular inclusion. *J Mech Phys Solids* 1964; 12: 177–189.
11. Comninou M and Schmeuser D. The interface crack in a combined tension–compression and shear field. *J Appl Mech* 1979; 46: 345–348.
12. Comninou M and Dundurs J. Effect of friction on the interface crack loaded in shear. *J Elast* 1982; 10(2): 203–212.
13. Comninou M and Chang FK. Effects of partial closure and friction on a radial crack emanating from a circular hole. *Int J Fract* 1985; 28: 29–36.
14. Erdogan F and Gupta GD. Layered composites with an interface flaw. *Int J Solids Struct* 1971; 7: 1089–1107.
15. Erdogan F, Gupta GD and Ratwani M. Interaction between a circular inclusion and an arbitrarily oriented crack. *J Appl Mech* 1974; 41: 1007–1013.
16. Hills DA and Comninou M. A normally loaded half-plane with an edge crack. *Int J Solids Struct* 1985; 21: 399–410.
17. Hills DA and Nowell D. Stress intensity calibrations for closed cracks. *J Strain Anal* 1989; 24: 37–43.
18. Hills DA, Kelly PA, Dai DN, et al. *Solution of crack problems-the distributed dislocation technique*. Dordrecht, The Netherlands: Kluwer Academic Publishers, 1996.
19. Jin X and Keer KL. Solution of multiple edge cracks in an elastic half plane. *Int J Fract* 2006; 137: 121–137.
20. Nowell D and Hills DA. Open cracks at or near free edges. *J Strain Anal* 1987; 22: 177–185.
21. Maheshwari M, Annamdas V, Pang J, et al. Crack monitoring using multiple smart materials; fiber-optic sensors & piezo sensors. *Int J Smart Nano Mater* 2017; 8(1): 41–55.
22. Liang YC and Hwu C. On-line identification of holes/cracks in composite structures. *Smart Mater Struct* 2001; 10: 599–609.
23. Hattori G and Sáez A. Crack identification in magnetoelectroelastic materials using neural networks, self-organizing algorithms and boundary element method. *Comput Struct* 2013; 125: 187–199.
24. Liang YC and Sun YP. Hole/crack identification in circular piezoelectric plates. *Proce Eng* 2014; 79: 194–203.
25. Hwu C and Liang YC. Hole/crack identification by static strains from multiple loading modes. *AIAA J* 2001; 39: 315–324.
26. Liang YC and Sun YP. Hardware-in-the-loop simulations of hole/crack identification in a composite plate. *Materials* 2020; 13: 424.
27. Chatzi E, Hiriyur B, Waisman H, et al. Experimental application and enhancement of the XFEM-GA algorithm for the detection of flaws in structures. *Comput Struct* 2011; 89: 556–570.
28. Rabinovich D, Givoli D and Vigdergauz S. XFEM-based crack detection scheme using a genetic algorithm. *Int J Numer Methods Eng* 2007; 71: 1051–1080.
29. Rabinovich D, Givoli D and Vigdergauz S. Crack identification by arrival time using XFEM and a genetic algorithm. *Int J Numer Methods Eng* 2009; 77: 337–359.

30. Waisman H, Chatzi E and Smyth AW. Detection and quantification of flaws in structures by the extended finite element method and genetic algorithms. *Int J Numer Methods Eng* 2010; 82: 303–328.

31. Gadala M and McCullough A. On the finite element analysis of inverse problems in fracture mechanics. *Eng Comput* 1999; 16: 481–502.

32. Galvanetto U and Violaris G. Numerical investigation of a new damage detection method based on proper orthogonal decomposition. *Mech Syst Signal Proce* 2007; 21: 1346–1361.

33. Khatir S and Abdel M. Fast simulations for solving fracture mechanics inverse problems using POD-RBF XIGA and Jaya algorithm. *Eng Fract Mech* 2019; 205: 285–300.

34. Lanata F and Grosso A. Damage detection and localization for continuous static monitoring of structures using a proper orthogonal decomposition of signals. *Smart Mater Struct* 2006; 15: 1811–1829.

35. Bäcker D, Ricoeur A and Kuna M. Sensor concept based on piezoelectric PVDF films for the structural health monitoring of fatigue crack growth. *Struct Durab Health Monit* 2011; 7: 1–22.

36. Xiong Z and Glisic B. An inverse elastic method of crack identification based on sparse strain sensing sheet. *Struct Health Monit*. Epub ahead of print 27 July 2020. DOI: 10.1177/1475921720939518.

37. Boukellif R and Ricoeur A. Parameter identification for cracks in elastic plate structures based on remote strain fields. *Int J Solids Struct* 2014; 51: 2123–2132.

38. Boukellif R and Ricoeur A. Identification of crack parameters and stress intensity factors in finite and semi-infinite plates solving inverse problems of linear elasticity. *Acta Mech* 2020; 231: 795–813.

39. Boukellif R and Ricoeur A. Detection of notches and cracks based on the monitoring of local strain and the solution of inverse problems. *Mater Design Proce Commun*. Epub ahead of print 14 August 2019. DOI: 101002/mdp2103.

40. Holland JH. *Adaptation in natural and artificial systems.* Cambridge: MIT Press, 1992.

41. Goldberg DE. *Genetic algorithms in search, optimization and machine learning.* Boston, MA: Addison-Wesley Publishing Company, 1989.